Sensitivity improvement and carrier power reduction in direct-detection optical OFDM systems by subcarrier pairing

Yi Hong, Arthur J. Lowery,* and Emanuele Viterbo

Department of Electrical & Computer Systems Engineering, Monash University, Clayton, VIC 3800, Australia
**arthur.lowery@eng.monash.edu.au*

Abstract: This paper introduces subcarrier pairing to optical OFDM systems and shows, using simulations, that the sensitivity of Direct-Detection Optical Orthogonal Frequency Division Multiplexed (DDO-OFDM) systems can be improved by 0.7 dB, without any coding overheads. Subcarrier pairing works because each subcarrier acquires a different electrical Signal to Interference plus Noise Ratio (SINR), which typically increases with the subcarrier's frequency. Pairing the good and bad subcarriers, so that information is split between them, improves the performance of the bad subcarrier more than it degrades the performance of the good subcarrier. This lowers the required Optical Signal to Noise Ratio (OSNR) for the system to give a certain Bit Error Ratio (BER).

©2012 Optical Society of America

OCIS codes: (060.4080) Modulation; (060.4510) Optical communications.

References and links

1. A. J. Lowery and J. Armstrong, "Orthogonal-frequency-division multiplexing for dispersion compensation of long-haul optical systems," Opt. Express **14**(6), 2079–2084 (2006).
2. B. J. C. Schmidt, Z. Zan, L. B. Du, and A. J. Lowery, "120 Gbit/s over 500-km using single-band polarization-multiplexed self-coherent optical OFDM," J. Lightwave Technol. **28**(4), 328–335 (2010).
3. W. Shieh and C. Athaudage, "Coherent optical orthogonal frequency division multiplexing," Electron. Lett. **42**(10), 587–588 (2006).
4. S. L. Jansen, I. Morita, N. Tadeka, and H. Tanaka, "20-Gb/s OFDM transmission over 4,160-km SSMF enabled by RF-pilot tone phase noise compensation," in *Conference on Optical Fiber Communication, OFC* (Anaheim, CA., 2007), p. PDP15.
5. A. J. Lowery, "Amplified-spontaneous noise limit of optical OFDM lightwave systems," Opt. Express **16**(2), 860–865 (2008).
6. S. L. Jansen, I. Morita, and H. Tanaka, "Carrier-to-signal power in fiber-optic SSB-OFDM transmission systems" in *IEICE General Conference* (Nagoya, 2007), pp. B-10–24, 363.
7. G. Raleigh and J. Cioffi, "Spatio-temporal coding for wireless communication," IEEE Trans. Commun. **46**(3), 357–366 (1998).
8. R. Knopp and G. Caire, "Power control schemes for TDD systems with multiple transmit and receive antennas," in *Proc. of IEEE Global Telecommunications Conference (Globecom)* (Rio de Janeiro, 1999), pp. 2326–2330.
9. S. K. Mohammed, E. Viterbo, Y. Hong, and A. Chockalingam, "MIMO precoding with X- and Y-codes," IEEE Trans. Inf. Theory **57**(6), 3542–3566 (2011).
10. J. Boutros and E. Viterbo, "Signal space diversity: a power- and bandwidth-efficient diversity technique for the Rayleigh fading channel," IEEE Trans. Inf. Theory **44**(4), 1453–1467 (1998).
11. Y. Hong, E. Viterbo, and A. J. Lowery, "Improving the sensitivity of direct-detection optical OFDM systems by pairing of the optical subcarriers," in *European Conference on Optical Communications* (Geneva, 2011), p. Th.11.B.2.
12. G. Caire, G. Taricco, and E. Biglieri, "Bit-interleaved coded modulation," IEEE Trans. Inf. Theory **44**(3), 927–946 (1998).
13. J. M. Tang, P. M. Lane, and K. A. Shore, "High-speed transmission of adaptively modulated optical OFDM signals over multimode fibers using directly modulated DFBs," J. Lightwave Technol. **24**(1), 429–441 (2006).
14. C. S. Park and K. B. Lee, "Transmit power allocation for BER performance improvement in multicarrier systems," IEEE Trans. Commun. **52**(10), 1658–1663 (2004).
15. Q. Yang, W. Shieh, and Y. Ma, "Bit and power loading for coherent optical OFDM," IEEE Photon. Technol. Lett. **20**(15), 1305–1307 (2008).

#155428 - $15.00 USD Received 28 Sep 2011; revised 15 Oct 2011; accepted 17 Oct 2011; published 11 Jan 2012
(C) 2012 OSA

16. B. Cardiff, M. F. Flanagan, F. Smyth, L. P. Barry, and A. D. Fagan, "On bit and power loading for OFDM over SI-POF," J. Lightwave Technol. **29**(10), 1547–1554 (2011).

1. Introduction

Direct-Detection Optical Orthogonal Frequency Division Multiplexing (DDO-OFDM) [1] was originally proposed as a method for efficient fiber dispersion compensation for long-haul transmission. In DDO-OFDM, a high-rate signal is encoded into many lower-rate signals, each modulated onto a separate subcarrier. The dispersion is equalized using a single phase shift applied to each subcarrier. DDO-OFDM has been studied extensively since its inception, and systems transmitting 120 Gbit/s per band of subcarriers have been demonstrated experimentally [2]. A parallel development to DDO-OFDM has been Coherent Optical OFDM (CO-OFDM) [3], which does not transmit the carrier, but instead uses a local-oscillator laser at the receiver. For this reason, CO-OFDM is more sensitive to the randomly-evolving relative phase between the transmitter and the laser, unless a pilot is used and mixed with the signal of the subcarriers before the receiver's FFT [4].

An advantage of CO-OFDM over DDO-OFDM is that requires around 7-dB less Optical Signal to Noise Ratio (OSNR) at the input to the receiver in order to attain the same Bit-Error Ratio (BER) at the receiver's output [5]. This is for three reasons: (1) DDO-OFDM requires a carrier to be transmitted with equal power to the subcarriers [6]; (2) with CO-OFDM electrical noise generated by the intermixing of the subcarriers and optical noise at the photodiode can be minimized, or eliminated with a balanced receiver; (3) electrical noise generated by noise mixing with itself can also be eliminated with a balanced coherent receiver. A modification to DDO-OFDM, where the carrier is sent, but then used as a local-oscillator in a coherent receiver ("Self-Coherent Optical OFDM") [2], reduces penalties (2) and (3), but at the expense of a far-more complex coherent receiver and the addition of a precise narrow-bandwidth optical filter. Thus it would be desirable to develop a DDO-OFDM system with an improved sensitivity, but without resorting to the complexity of a coherent optical receiver.

In DDO-OFDM, all the subcarriers can be treated as parallel subchannels. Moreover, an interesting feature of the electrical noise spectrum of DDO-OFDM is that theoretically the noise decreases at higher frequencies. This is due to the subtleties of the intermixing of the optical noise spectrum with the subcarrier spectrum, which were illustrated in a previous paper [5]. Thus the higher-frequency subcarriers should, in theory, offer a better BER performance than the lower-frequency subcarriers, i.e., subcarriers transmit signals under unbalanced signal to interference and noise ratios (SINRs).

The above scenario is very similar to multiple-input multiple-output (MIMO) wireless systems using singular value decomposition (SVD) precoding [7,8]. After SVD processing, the MIMO channels are transformed into parallel subchannels with different signal to noise ratios (SNRs). Pairing of the subchannels can then be used to further improve the BER performance [9]. In particular, subchannels with different SINRs and different diversity gains are paired together. A pair of subchannels is then jointly pre-coded using signal constellation rotations and component interleaving [10]. The essential idea is to make the real and imaginary components of the received symbols affected by two independent channel fading coefficients. If one channel loses one component due to deep fading, the other component is still valid. This will offer modulation diversity gain, or equivalently, is more robust against the effect of noise. Such a pairing scheme has been successfully explored for wireless MIMO in [9]. However, it has not yet been explored for optical OFDM, as the dependence of noise on subcarrier frequency is a subtle feature of DDO-OFDM.

Motivated by the above, in this paper we first derive the analytical expression of electrical power spectral density (PSD) and show that it matches a system simulation including optical amplifier noise. This analysis enables us to exactly compute the SINR in each subcarrier without the need of simulations. We then exploit the idea of *subcarrier pairing*, i.e., information is pre-coded across two subcarriers with unbalanced SINRs by using a complex

#155428 - $15.00 USD Received 28 Sep 2011; revised 15 Oct 2011; accepted 17 Oct 2011; published 11 Jan 2012
(C) 2012 OSA

exponential factor parameterized by a single angle and component interleaving. The angle can be optimally selected for the different subcarrier pairs. Since joint pre-coding is performed only across a pair of subcarriers, the complexity of joint maximum likelihood detection (MLD) is low.

We report the optimal angles and we show, using Monte-Carlo simulations, that pairing subcarriers can improve the receiver sensitivity of a DDO-OFDM in terms of OSNR. This is because the BER of a system is dominated by the errors in its worst subcarriers; and pairing reduces these errors. The skewed noise spectrum after photodetection is mainly due to subcarriers mixing with the Amplified Spontaneous Emission (ASE) noise, so a high-power carrier is beneficial to reduce this contribution of electrical noise relative to the carrier mixing with the optical noise. Pairing allows the carrier power to be reduced from this optimum. The reduction of the carrier's power effectively assigns more power to the subcarriers for a given OSNR, further improving the sensitivity of the system.

This work is an extension of the paper presented at the European Conference on Optical Communications, Geneva, in September 2011 [11]. Full details of the analytical model used to determine the SINRs are included, and additional results using VPItransmissionMaker to simulate the pairwise system with an optical noise generator are presented to confirm the previous MATLAB results which were based on stochastic electrical noise generator. A discussion on the interaction of Subcarrier Pairing and Forward-Error Correcting (FEC) codes has also been added.

2. System model

Figure 1 shows a diagram of the complete system, including pairwise coding. For this part of the discussion, we shall ignore the Rotate and MLD blocks. The complete system is as described in Ref. [1]. For each OFDM symbol, data bits are coded as 4-QAM, then collected as a vector and sent to an inverse Fast Fourier Transform (FFT). This generates a time-waveform, which is a superposition of QAM modulated subcarriers. A Cyclic Prefix (CP) is usually added to each OFDM symbol, to accommodate symbol-spreading due to dispersion without a penalty. The resulting OFDM symbol is converted to inphase (I) and quadrature (Q) analog waveforms using Digital-to-Analog Converters (DACs). Inphase and quadrature components of a high-frequency carrier are added to the I and Q waveforms, to create a virtual carrier by frequency-down-shifting the laser line by $B_{gap} + B_{sc}/2$. These waveforms drive a complex optical modulator to create the DDO-OFDM spectrum shown in the inset. This is transmitted over an amplified optical link, which adds ASE. The bandwidth of the ASE is limited by an optical bandpass filter. The photodetector causes intermixing of the carrier, ASE and subcarriers, as will be discussed below. A pair of microwave mixers down-convert the electrical spectrum so that the subcarriers lie either side of DC (the subcarrier at DC is not used for data transmission); this means that lower-rate Analog-to-Digital Converters (ADCs) can be used. The CP is stripped from the signal. An FFT acts as a matched filter for all of the subcarriers, producing a complex number for each subcarrier. Phase offsets are added to each subcarrier to equalize the phase distortion accumulated along the link, chiefly due to chromatic dispersion. In a typical DDO-OFDM system, a QAM demodulator follows the equalizer, slicing the complex signal to recover the data bits. This process is repeated for each OFDM symbol to give continuous data transmission. The equalizer is trained at the beginning of a simulation run by sending a data sequence known to the receiver under noiseless conditions and comparing the phases and magnitudes of the received subcarriers with their transmitted values.

#155428 - $15.00 USD Received 28 Sep 2011; revised 15 Oct 2011; accepted 17 Oct 2011; published 11 Jan 2012
(C) 2012 OSA

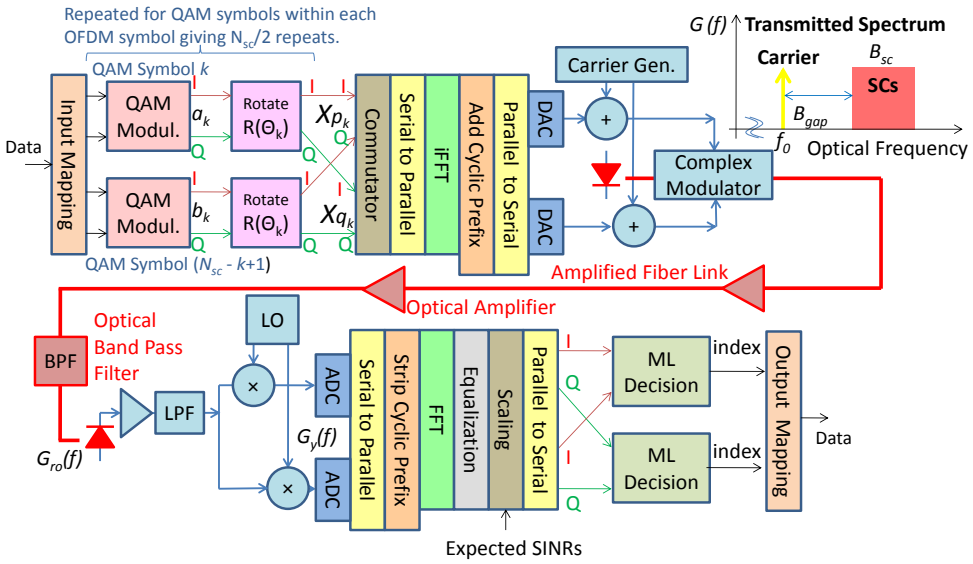

Fig. 1. Direct detection optical OFDM schematic. The Rotate, Scaling and ML Decision blocks are new additions to standard DDO-OFDM systems. Note the peculiar mapping of the I and Q signals from the Rotate block to the commutator, which is needed to realize component interleaving.

3. Electrical noise and interference spectrum

If the received subcarriers all possessed the same SINR, then there would be no point in using pairwise coding. However, the SINR is frequency dependent, even for a flat ASE spectrum. This is because of the details of the mixing that occurs at the photodetector, which is a square-law device, which outputs a photocurrent proportional to the square of the optical field it receives as input. Here we split the output current into its non-trivial components to deduce the form of the SINR's variation with frequency.

Following the notation in Reference [5], N_{sc} is the number of subcarriers in the DDO-OFDM, occupying the bandwidth B_{sc}. As illustrated at the top of Fig. 2, B_{gap} is the guard band's width between the optical carrier and the lowest frequency subcarrier, and B_{ASE} is the overall ASE noise bandwidth. Finally, B_L and B_H are the lower and upper excess noise bands. In the time domain, the received optical signal is given by

$$r_0(t) = s(t) + A\cos(2\pi f_0 t) + n_h(t) + n_v(t) \tag{1}$$

where: $n_h(t)$ and $n_v(t)$ denote the ASE noise in the horizontal and vertical polarizations, which are assumed equal in power (unpolarized noise). We assume the optical signal $s(t)$ and the optical carrier at frequency f_0 are sent on the horizontal polarization. The signal $s(t)$ represents the transmitted optical OFDM subcarrier band, i.e.

$$s(t) = \mathrm{Re}\left(\sum_{k=0}^{N_{sc}-1} X_k e^{j2\pi(f_0 + B_{gap} + k\Delta f)t} \right) \tag{2}$$

where: X_k are complex M-QAM symbols with average energy E_x and $\Delta f = B_{sc}/N_{sc}$ is the frequency spacing of the subcarriers.

Figure 2 shows the double sided PSD of the received optical signal $r_0(t)$ on a linear scale, denoted by $G_{ro}(f)$. $P_{ca} = A^2/2$ is the power of the optical carrier and $P_s = 2S_0B_{sc}$ is the total power in the OFDM subcarriers for continuous signals. For discrete signals, we define $P_{sc} = 2S_0\Delta f$, so that we can write $P_s = N_{sc}P_{sc}$. Finally, $\eta = P_{ca} / P_s$ is the carrier-to-signal power ratio.

#155428 - $15.00 USD Received 28 Sep 2011; revised 15 Oct 2011; accepted 17 Oct 2011; published 11 Jan 2012
(C) 2012 OSA

We define OSNR in the standard way as the total optical signal power (P_{ca} + P_s), divided by the ASE noise power in both polarizations, falling within the standard reference bandwidth of 12.5-GHz (0.1 nm at 1550 nm). Using an optical filter and direct detection by a photodiode with responsivity R, we obtain the down-converted electrical current

$$y(t) = R\left(\left|s(t) + A\cos(w_c t) + n_v(t)\right|^2 + \left|n_h(t)\right|^2\right). \tag{3}$$

Because both the signal and noise scale with responsivity (there is no photodiode or electrical noise considered in the derivations), we will assume unit responsivity for the following derivations to simplify the equations.

4. Electrical PSD and SINRs of DDO-OFDM

The analytical expression of the electrical PSD follows from (3) as

$$\begin{aligned} G_y(f) = &\underbrace{2G_s(f) * \frac{A^2}{4}\left[\delta(f - f_0) + \delta(f + f_0)\right]}_{\{1\}} + \underbrace{G_s(f) * G_s(f)}_{\{2\}} + \underbrace{G_n(f) * G_n(f)}_{\{3\}} \\ &+ \underbrace{2G_n(f) * \frac{A^2}{4}\left[\delta(f - f_0) + \delta(f + f_0)\right]}_{\{4\}} + \underbrace{2G_s(f) * G_n(f)}_{\{5\}} + [DC, 2f_0 \text{ component}] \end{aligned} \tag{4}$$

where * denotes the convolution operation and $\delta(f)$ the Dirac function. The terms $G_s(f)$ and $G_n(f) = N_{ASE}$ are the PSD of the OFDM signal $s(t)$ and of the ASE noise in both polarizations, respectively. The above expression is valid under the assumption that both $n(t)$ and $s(t)$ are zero-mean Gaussian random processes with variances N_{ASE} and S_0, respectively. This assumption is valid when the number of subcarriers is sufficiently large.

In Eq. (4), term {1} contains the power spectrum of the useful OFDM signal which has been down-converted by the subcarriers mixing with the carrier upon photodetection; {2} is the autocorrelation of $G_s(f)$ accounting for the unwanted tones [5]; {3} is the autocorrelation of $G_n(f)$; {4} is noise that has been down converted by mixing with the carrier; and {5} comes from mixing of noise with the OFDM subcarriers. The sum of the terms {2}, {3}, {4} and {5} represents the noise and interference impairments. The DC component stems from the optical carrier and the unwanted tones, while the ($2f_0$) stems from the optical carrier. It is important to note that some of the resulting baseband components are generated from the negative frequency parts of the underlying double-sided PSDs. The electrical signal $G_y(t)$ is further processed by a low pass filter (LPF) with cutoff frequency B_{gap} + B_{sc} + B_H, and its DC component is removed. The corresponding filtered terms in Eq. (4) are shown in Fig. 2 on a linear scale by analytic computation of the continuous convolution operations. In practice, a spectrum analyzer in a simulation will operate on sampled signals and display sampled spectra with a given resolution bandwidth B_{res}. The corresponding convolution operations are replaced by discrete convolutions of sampled spectra.

Figure 3 shows that the electrical PSDs given by Eq. (4) match those computed by VPItransmissionMaker. The RF noise floor was obtained by simulating four identical OFDM symbols, which means that the subcarrier has no power in 3 out of 4 of the computed frequency bins, so the noise floor can be observed. In this comparison, the *one sided* PSD (where positive frequency PSDs in Fig. 1(b) are scaled by a factor two) is shown on a logarithmic scale. In this example, we consider a 60 Gbit/s optical OFDM signal using 4-QAM modulation with 1024 bits per OFDM symbols using N_{sc} = 512 subcarriers. The OFDM signal occupies B_{sc} = 30 GHz bandwidth. A gap, B_{gap} = 30 GHz, between the carrier and the subcarriers was used. The total ASE noise bandwidth is B_{ASE} = 60 GHz. The resolution bandwidth $B_{res} = \Delta f/4$ = 14.648 MHz. The optical power into the photodiode is 1 mW and the photodiode has a responsivity of 1 A/W with the RF power measured into a load of 1 Ω. The

#155428 - $15.00 USD Received 28 Sep 2011; revised 15 Oct 2011; accepted 17 Oct 2011; published 11 Jan 2012
(C) 2012 OSA

RF powers of the signals and noise all scale with the square of the optical power and responsivity, but linearly with the load resistance. Note that, because the resolution bandwidth is one-quarter of the subcarrier spacing, the indicated SINR (the difference between the red and black lines) is 6 dB more than the actual SINR that a subcarrier would experience. Thus, we would expect a SINR in the range 6 dB to 9 dB for 13-dB OSNR.

Thanks to the frequency guard band B_{gap} = 30 GHz, the unwanted intermodulation tones can be ignored [1] as they fall at frequencies below the wanted subcarriers. The wanted subcarriers each have a different electrical $SINR_i$, $i = 1,\ldots, N_{sc}$, defined as the ratio of power of OFDM signal at the *i*-th subcarrier and the noise and interference power at the *i*-th subcarrier, measured over a bandwidth equal to the subcarrier spacing. This is due to the noise and interference impairments shown in Fig. 2. The analytical results of Eq. (4) allow each $SINR_i$, to be computed without the need for Monte-Carlo simulations. The computed SINRs are shown in Fig. 4 for OSNR = 10, 13, 15 and 19 dB. The electrical SINR increases at higher frequencies, due the contributions of *ASE* × *ASE* noise and *ASE* × *subcarrier* noise, which are both frequency dependent (see Fig. 2). For 10-dB OSNR, the increase is 4 dB: for 19-dB OSNR this reduces to 3.2 dB. This difference is due to the relative contribution of *ASE* × *ASE* noise. For high OSNRs, *ASE* × *ASE* noise is negligible and so contributes to the slope in SINR across the band only marginally.

#155428 - $15.00 USD Received 28 Sep 2011; revised 15 Oct 2011; accepted 17 Oct 2011; published 11 Jan 2012
(C) 2012 OSA

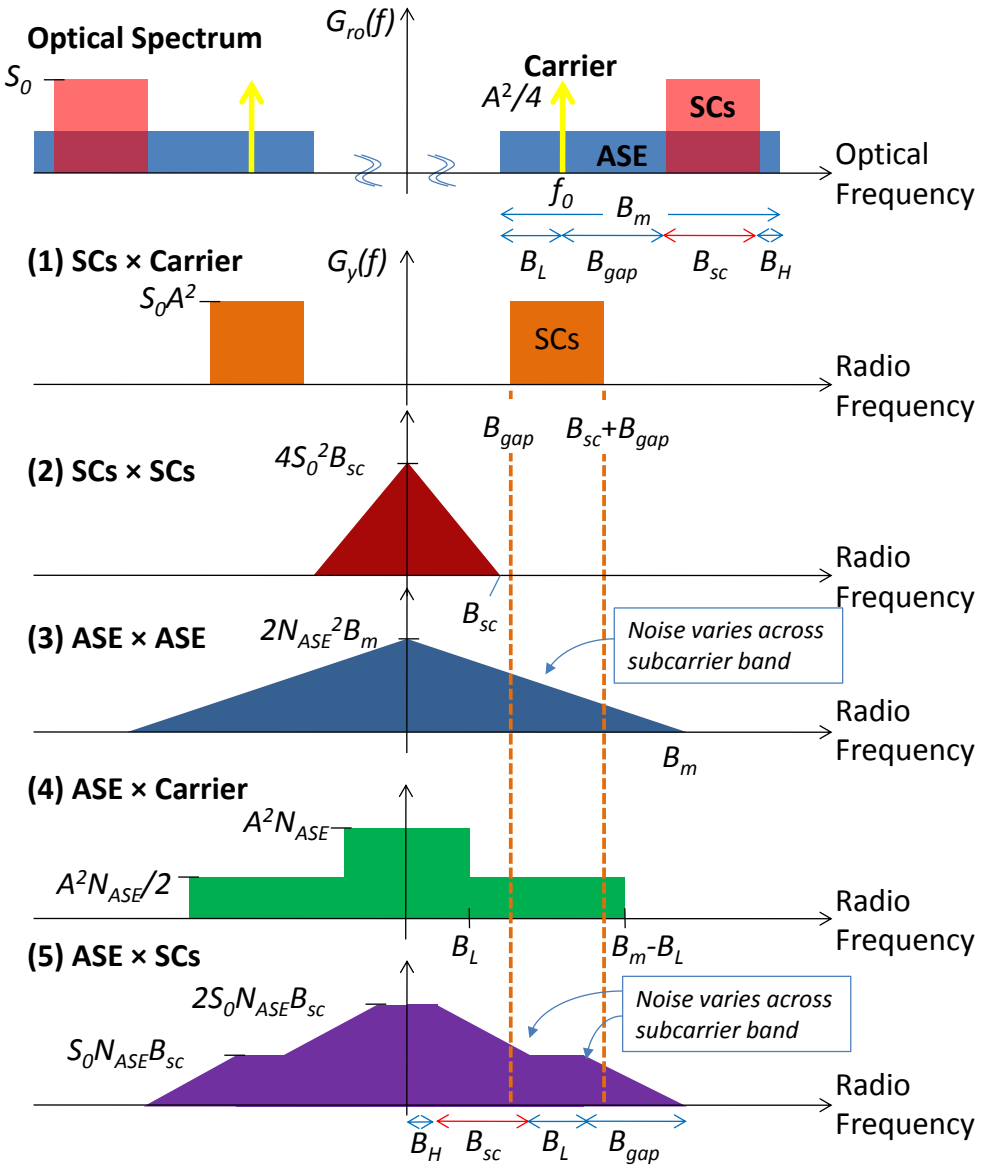

Fig. 2. The received optical spectrum (top) with the components of the RF spectrum that are created upon photodetection (1-5).

#155428 - $15.00 USD Received 28 Sep 2011; revised 15 Oct 2011; accepted 17 Oct 2011; published 11 Jan 2012
(C) 2012 OSA

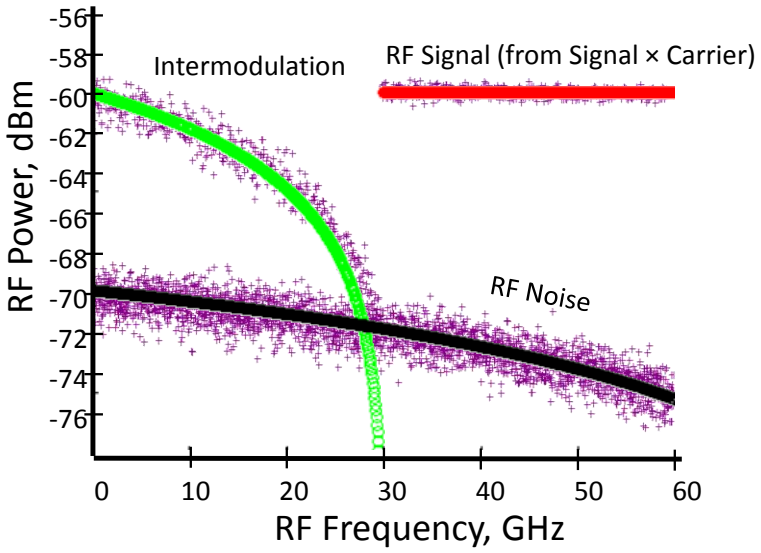

Fig. 3. Simulated (crosses) and analytical RF signal and noise levels (lines). Note that the RF noise level drops at higher frequencies. $\eta = 1.0$, OSNR = 13 dB, $B_L = B_H = 0$, $B_{ASE} = 60$ GHz.

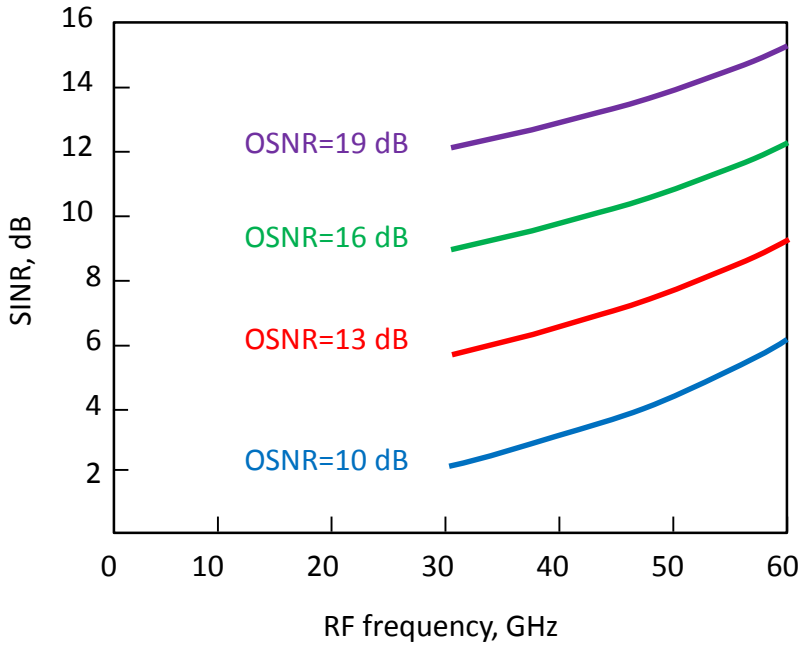

Fig. 4. Variation of Signal to Interference Noise Ratio (SINR) across the subcarrier band for a number of OSNRs.

5. DDO-OFDM with pairing of "good" and "bad" subcarriers

Reference [9] showed that in a wireless MIMO system the quality and reliability can be enhanced by coding the signal such that each of the two subcarriers in a pair is modulated with some of the original information from each the individual subcarriers. The level of

#155428 - $15.00 USD Received 28 Sep 2011; revised 15 Oct 2011; accepted 17 Oct 2011; published 11 Jan 2012
(C) 2012 OSA

mutual information is determined according to the SINR; the information exchange is implemented by swapping the I and Q components of the pair after their constellations have been rotated. We can exploit the same concept to improve the OSNR requirements of DDO-OFDM. We consider the set of pairs $\Psi = \{(p_k,q_k), k = 1,\ldots,N_{sc}/2\}$ forming a *partition* of the N_{sc} subcarriers, where k is the index of pairs. According to [9], good subcarriers with high SINR should be paired with bad subcarriers with low SINR, so that the pairing of the corresponding subcarriers should be [9]: $S = \{(p_k, q_k) = (k, N_{sc} - k + 1), k = 1,\ldots, N_{sc}/2\}$. As a simple example, if the system had 6 overall subcarriers ($N_{sc} = 6$), we would have three pairs of subcarriers. The first pair ($k = 1$), would include the 1st and the 6th subcarriers, i.e., $(p_1,q_1) = (1, 6)$. The second pair ($k = 2$), will include the 2nd and the 5th subcarriers, i.e., $(p_2,q_2) = (2, 5)$. The last pairing ($k = 3$) will be $(p_3,q_3) = (3, 4)$.

The actual coding is performed across a pair (indexed by k) of M-QAM information symbols a_k and b_k (see Fig. 1) by multiplying by rotation factor $e^{j\theta_k}$, yielding two rotated complex symbols $a_k e^{j\theta_k}$ and $b_k e^{j\theta_k}$, where θ_k is the *rotation angle* for the k-th pair. The impact of the rotation angle on the error performance of MIMO systems has been discussed in [9] and the optimal rotation angle, denoted by θ_k^{opt}, was derived analytically for 4-QAM, to minimize the total error probability and is given by

$$\theta_k^{opt} = \begin{cases} \pi/4 & \beta_k \le \sqrt{3} \\ \tan^{-1}\left[(\beta_k^2 - 1) - \sqrt{(\beta_k^2 - 1)^2 - \beta_k^2}\right] & \beta_k > \sqrt{3} \end{cases} \tag{5}$$

where $\beta_k = \lambda_{q_k} / \lambda_{p_k}$ is called *condition number* of the pair of subcarriers (p_k, q_k), and

$$\lambda_{p_k} = \sqrt{SINR_{p_k}} \quad ; \quad \lambda_{q_k} = \sqrt{SINR_{q_k}} \quad . \tag{6}$$

The condition number describes the SINR imbalance between the two subcarriers. Figure 5 plots the optimum rotation angle for $\eta = 0.5$. For higher OSNRs, there are fewer subcarrier pairs with optimal rotation angles θ_k^{opt} that are not 45°. Specifically, when OSNR = 7 and 19 dB, there are 54 and 6 subcarrier pairs whose condition number is greater than $\sqrt{3}$, respectively.

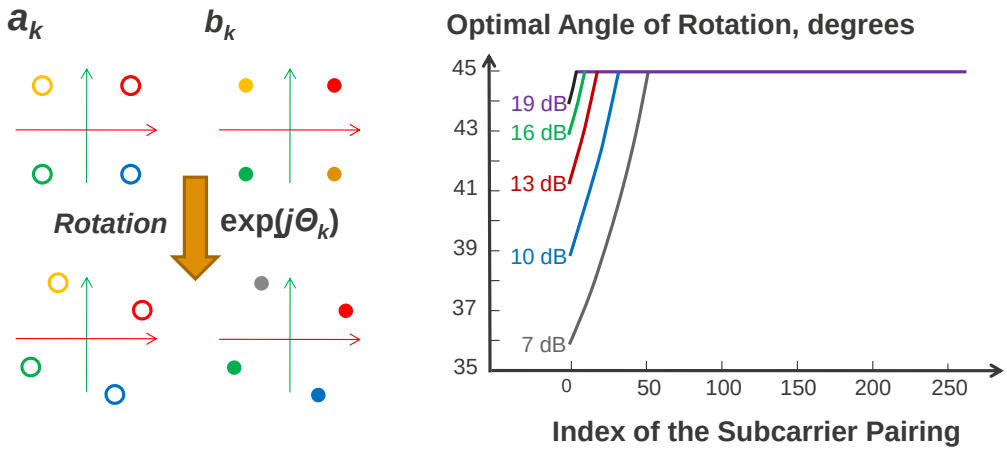

Fig. 5. Optimal angle of pairing versus the index of subcarrier pairing. The higher-frequency subcarriers have a 45-degree optimum. The label is OSNR.

#155428 - $15.00 USD Received 28 Sep 2011; revised 15 Oct 2011; accepted 17 Oct 2011; published 11 Jan 2012
(C) 2012 OSA

After rotation, IQ component interleaving is used over the two precoded symbols, $a_k e^{j\theta_k}$ and $b_k e^{j\theta_k}$. The IQ component interleaver described in [10] exchanges the real part of $b_k e^{j\theta_k}$ and the imaginary part of $a_k e^{j\theta_k}$, to obtain two transmitted complex symbols:

$$X_{p_k} = \mathrm{Re}(a_k e^{j\theta_k}) + j\,\mathrm{Re}(b_k e^{j\theta_k}); \quad X_{q_k} = \mathrm{Im}(a_k e^{j\theta_k}) + j\,\mathrm{Im}(b_k e^{j\theta_k}) \qquad (7)$$

where Re and Im denote the real and imaginary parts of a complex symbol. Component interleaving is illustrated in Fig. 6 for symbols that have been rotated by 45 degrees.

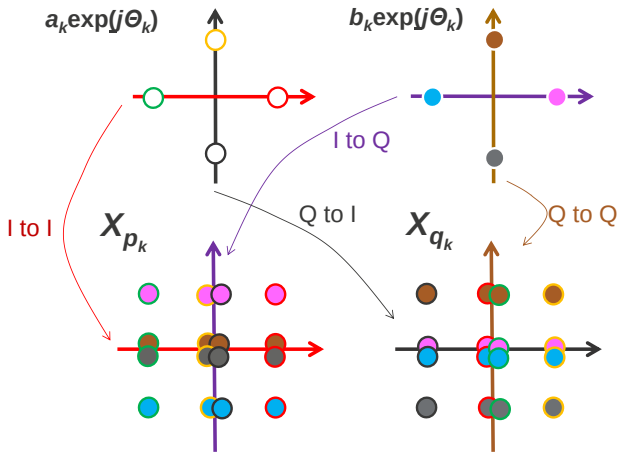

Fig. 6. Illustration of component interleaving on symbols that have been rotated by 45°. The color coding is significant as it shows how an output symbol's position is determined by the positions of two input symbols. The output symbols X have been slightly displaced (for example, at the origin), to show that multiple symbols from the original constellations can map to a single point on the interleaved constellations. Nine constellation points are created for 45° rotation. For rotations of less than 45°, sixteen constellation points will be created.

After transmission and photodetection, the symbol pairs (p_k, q_k) will acquire different SINRs with the difference in SINR dependent on the index of the pair, k. In order to apply ML detection correctly, the constellations after component de-interleaving should have circularly symmetric spreads. This can be achieved by scaling each received symbol by the square-root of its expected SINR before component de-interleaving; that is, symbols with low SINRs are reduced in size relative to the symbols with higher SINRs. Figure 7 illustrates this process.

#155428 - $15.00 USD Received 28 Sep 2011; revised 15 Oct 2011; accepted 17 Oct 2011; published 11 Jan 2012
(C) 2012 OSA

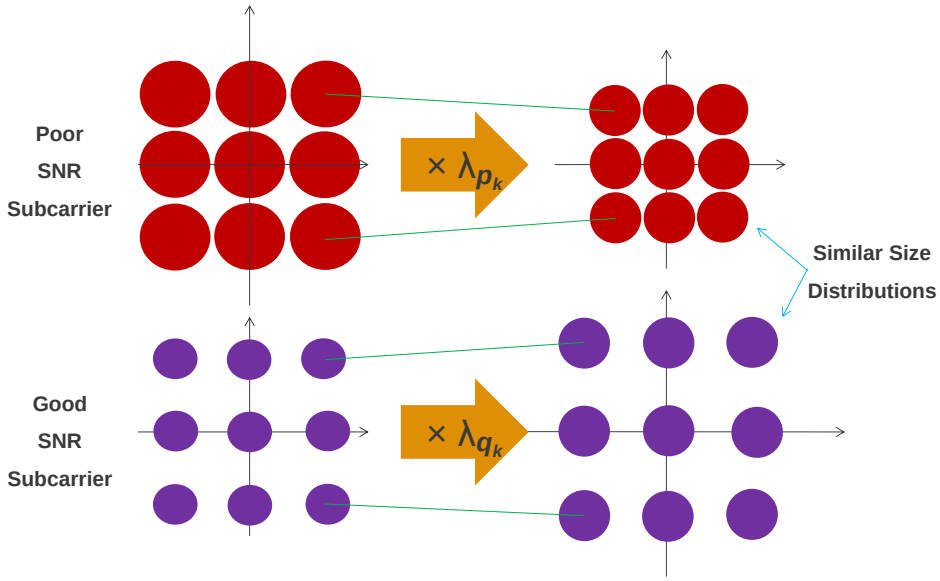

Fig. 7. Illustration scaling to produce constellations with similar-sized distributions.

Figure 8 illustrates component de-interleaving of the scaled constellations of Fig. 7. In this illustration, the new constellation (upper right) is formed from the real values of the points in the pair of symbols, similar to component interleaving. The imaginary values of the original pair can also be used to form a new symbol (lower right). Because the received constellations have been scaled, the new constellation loses its $\pi/2$ rotational symmetry. Note that because the distributions of the original pair of symbols have been scaled to have equal size, the distributions in the de-interleaved constellation are circularly symmetric.

Finally, ML detection is used to determine which of the transmitted symbols each received symbol is closest to. This is illustrated in Fig. 9. Note that the candidate symbols are scaled by the appropriate root-SINRs in the real and imaginary directions. ML detection simply calculates the distance to each candidate symbol from the received symbol, then finds the argument of the minimum distance. The argument carries the values of the original data bits. An identical result could be achieved by applying the thresholds shown in green to the received constellation.

In both the encoding and the decoding process, constellation rotation and component interleaving both play important roles. The details on using constellation rotations and the IQ component interleaving/deinterleaving can be found in [10]. The idea is to make the real and imaginary components of the deinterleaved symbols affected by the two independent channel coefficients. For example, to decode a_k, if one channel loses one component, say $\mathrm{Re}(X_{p_k})$, due to a small coefficient λ_{p_k}, the other component $\mathrm{Re}(X_{q_k})$ is still valid and available to be decoded. This provides modulation diversity gain, or equivalently, more protection on decoding against the effect of noise [10].

#155428 - $15.00 USD Received 28 Sep 2011; revised 15 Oct 2011; accepted 17 Oct 2011; published 11 Jan 2012
(C) 2012 OSA

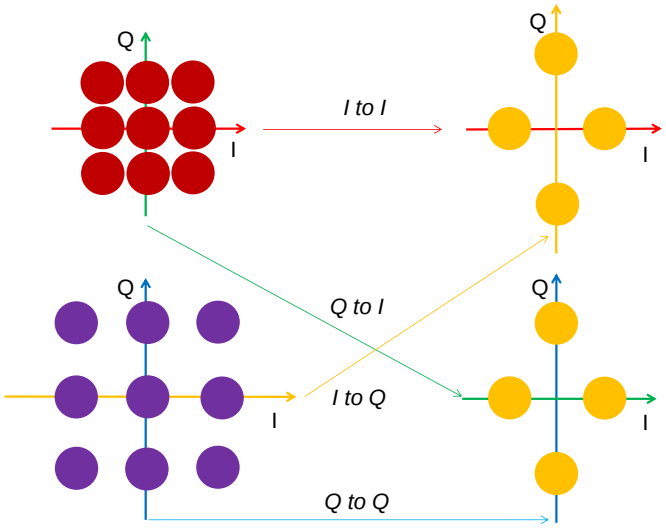

Fig. 8. Component de-interleaving. In this example, the inphase (real) values of a pair of symbols are used to create the upper new symbol: the quadrature (imaginary) values of two symbols are used to create the lower new symbol. The upper and lower new symbols are then passed to the upper and lower ML detectors, as shown in Fig. 1.

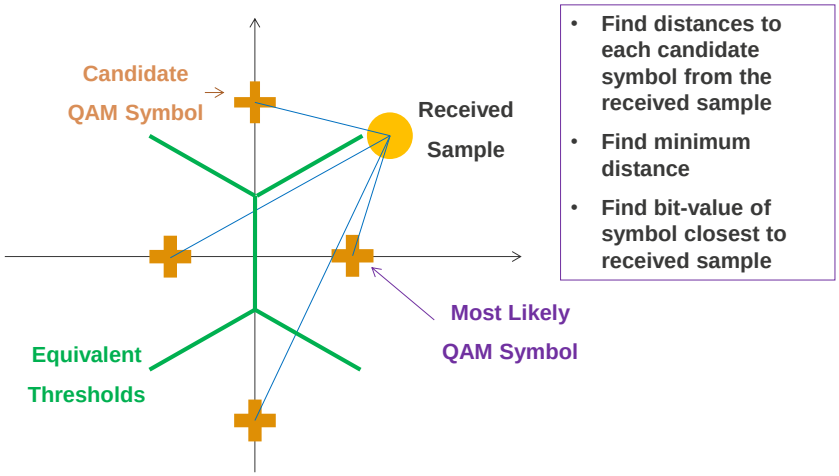

Fig. 9. Maximum Likelihood (ML) Detection process in each decoder (upper and lower). This is applied to every received symbol. The Equivalent Thresholds (green) are not used in the ML process, but are included to illustrate that there is not a simple pair of straight-line thresholds that can be used.

6. Simulations of the required OSNR with and without pairing

Figure 10 compares the OSNRs at which the systems can achieve BER of 10^{-3} as a function of the carrier-to-signal power ratio, η. These results were obtained using MATLAB® Monte-Carlo simulations of the receiver with the variance of the random electrical noise for each subcarrier set by the calculated SINR. To obtain each point, the OSNR was swept to obtain a plot of BER versus ONSR. Also included are points (◊) obtained using a VPItransmissionMaker simulation, where optical noise is added before the photodiode, so the photodetection generates electrical noise with the expected spectrum. These points validate the MATLAB model's results and confirm the quality of the Gaussian approximation of the

#155428 - $15.00 USD Received 28 Sep 2011; revised 15 Oct 2011; accepted 17 Oct 2011; published 11 Jan 2012
(C) 2012 OSA

interference terms. In the VPItransmissionMaker simulations, the rotation angle was fixed to 45°, which gives slightly suboptimal results.

When pairing is added to the MATLAB and VPItransmissionMaker simulations, the required OSNR is reduced over a wide range of carrier to subcarrier power ratios. If the carrier power is equal to the subcarrier power, the required OSNR can be reduced by 0.5 dB; however, pairing produces its best performance when the carrier power is lowered to 60% of the subcarrier power. This reduces the required OSNR by a further 0.2 dB.

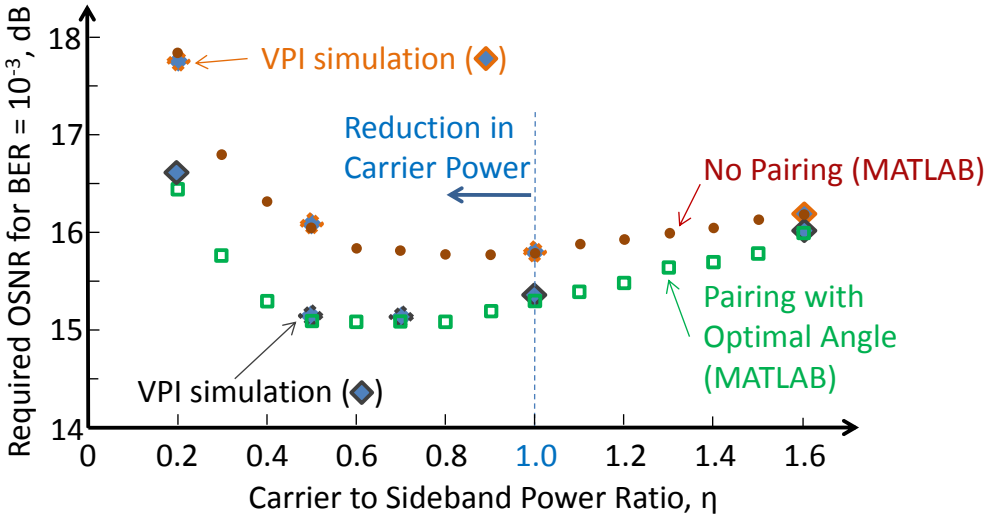

Fig. 10. Required OSNR for BER = 10^{-3} versus the ratio of carrier power to sideband power with and without pairing.

7. Discussion and conclusions

This paper has demonstrated that pairwise coding is beneficial to direct-detection optical OFDM systems, giving a performance 0.7 dB gain in a system where the subcarriers have a 3.2 dB difference in SINR across the band. Such a gain was also observed when the carrier power is less than the sideband power, which is potentially useful in reducing the effects of fiber nonlinearity. Pairing requires no coding overhead (it is a *Rate* = 1 code), so does not adversely impact on the spectral efficiency of the system. The results are also applicable to any optical OFDM system where subcarriers with bad SINR can be paired with subcarriers of good SINRs.

An open question is whether Subcarrier Pairing will give a gain in addition to conventional *Rate*<1 Forward-Error Correction (FEC) codes, or whether the FEC will itself compensate for mismatched SINRs. A full answer is left to a future paper; however, it is likely that the Subcarrier Pairing will give its coding gain in addition to the conventional FEC, provided that the errors provided to the FEC decoder are uncorrelated. Any correlation of errors could be cancelled by using "bit interleaved coded modulation" (BICM) techniques [12]: a bit interleaver could be placed between the FEC coder and the Subcarrier Pairing at the transmitter, and a bit deinterleaver between the MLD and the FEC decoder at the receiver.

It is interesting to compare pairwise coding with other techniques to cope with unequal subcarrier SINRs. Adaptive Modulation has been applied to optical OFDM for multimode fiber links, where the channel response fluctuates widely due to interference between the multiple propagation modes and the noise is flat and signal independent, as it is dominated by the receiver's electrical noise [13]. Adaptive Modulation in its simplest form, uses different constellation sizes (*e.g.* BPSK, QPSK, 8-QAM, 16-QAM) depending on the SINR of a

#155428 - $15.00 USD Received 28 Sep 2011; revised 15 Oct 2011; accepted 17 Oct 2011; published 11 Jan 2012
(C) 2012 OSA

particular subcarrier. It is suitable when the SINRs vary by at much more than 3 dB, which is not the case in our situation. Adaptive Modulation also varies the transmission rate of the channel, which is generally inconvenient in most telecommunications applications. Another technique to cope with unequal SINRs is to vary the transmission powers of subcarriers to equalize the error rates across the subcarriers ('Power Loading' [14]). Power loading may be very difficult to optimize, because in our situation the SINR depends on the subcarrier powers in a complex manner (due to the intermixing of the optical subcarriers with the broadband ASE noise). Combinations of bit and power loading are also possible [15, 16] and it is left to another paper to compare these with pairwise coding.

Acknowledgments

This work is supported under the Australian Research Council's Discovery funding scheme (DP1096782). We thank VPIphotonics for the use of their simulator, VPItransmissionMaker version 8.5.

#155428 - $15.00 USD Received 28 Sep 2011; revised 15 Oct 2011; accepted 17 Oct 2011; published 11 Jan 2012
(C) 2012 OSA